FLUORESCENT DETECTION OF SECONDARY STRUCTURE IN PANCREATIC CANCER

A Paper
Submitted to the Graduate Faculty
of the
North Dakota State University
of Agriculture and Applied Science

By

Aaron Bauer

In Partial Fulfillment of the Requirements
for the Degree of
MASTER OF SCIENCE

Major Program:
Biomedical Engineering

April 2022

Fargo, North Dakota

North Dakota State University
Graduate School

Title

FLUORESCENT DETECTION OF SECONDARY STRUCTURE IN PANCREATIC CANCER

By

Aaron Bauer

The Supervisory Committee certifies that this ***disquisition*** complies with North Dakota State University's regulations and meets the accepted standards for the degree of

MASTER OF SCIENCE

SUPERVISORY COMMITTEE:

Dr. Dali Sun
Chair

Dr. Annie Tangpong

Dr. Ali Alshami

Approved:

04/05/2022
Date

Dr. Benjamin Braaten
Department Chair

ABSTRACT

Pancreatic cancer has one of the highest mortality rates among all cancers largely due to the late-stage onset of symptoms and the lack of early detection methods. Extracellular vesicles (EVs) could serve the potential as the next biomarker for pancreatic cancer detection because they directly reflect the state and composition of their parent cells. This work aimed to generate a high-throughput assay by combining immunoprecipitation of EVs with β-sheet staining by Thioflavin T (ThT) in a 96-well plate based off previous findings that ThT could be used to measure the elevated β-sheet richness found in tumor-derived EVs. This research tested four different immunoprecipitation methods in a 96-well plate. Although this work was not able to successfully create a high-throughput assay, it offers insight to increase fluorescent sensitivity by using a fluorescent microscope and optimizing immunocapture of EVs by developing an improved mixing method in 96-well plate.

ACKNOWLEDGMENTS

I would like to thank my advisor Dr. Dali Sun for all allowing me to use his laboratory and resources along with his guidance and support. I would also like to thank Dr. Annie Tangpong and Dr. Ali Alshami for serving on my committee and providing insight and feedback on this paper.

DEDICATION

I dedicate this work to my fiancée, Kalaina, for always being by my side and continuing to push me to be a better person. Also, to my parents, Ken and Sheila, for their never-ending support.

TABLE OF CONTENTS

ABSTRACT iii

ACKNOWLEDGMENTS iv

DEDICATION v

LIST OF TABLES viii

LIST OF FIGURES ix

LIST OF ABBREVIATIONS x

LIST OF SYMBOLS xi

INTRODUCTION 1

BACKGROUND 3

Pancreatic Cancer 3

Extracellular Vesicles 5

Protein Secondary Structure 6

β-Sheet and Thioflavin T 6

METHODS 8

Cell Lines and Culture 8

Extracellular Vesicle Isolation from Culture Media 8

Fluorescent Spectroscopy 8

Immunoprecipitation and Thioflavin T Staining in a Centrifuge Tube 9

Immunoprecipitation and Thioflavin T Staining in a 96-Well Plate 9

RESULTS 11

Thioflavin T Verification 11

96-Well Plate Immunoprecipitation 12

DISCUSSION 15

CONCLUSION 18

REFERENCES 19

LIST OF TABLES

Table Page

1. Comparison of methods for protein secondary structural analysis 6

LIST OF FIGURES

Figure Page

1. Thioflavin T fluorescent intensity of previously developed assay and cell culture samples. 11

2. Scatter plot and linear regression of protein sample gradients and different well plate volumes. 12

3. Schematic of immunoprecipitation with Thioflavin T fluorescent staining. 13

4. Thioflavin T fluorescent intensity of different 96-well immunoprecipitation methods. 14

LIST OF ABBREVIATIONS

CA19-9	Carbohydrate Antigen 19-9
CD	Circular Dichroism
DNA	Deoxyribonucleic Acid
EpCAM	Epithelial Cell Adhesion Molecule
EVs	Extracellular Vesicles
FT-IR	Fourier Transform Infrared
µg	Microgram
µL	Microliter
µM	Micromolar
miRNA	Micro Ribonucleic Acid
mg	Milligram
mL	Milliliter
ng	Nanogram
nm	Nanometer
PDAC	Pancreatic Ductal Adenocarcinoma
PCR	Polymerase Chain Reaction
RNA	Ribonucleic Acid
ThT	Thioflavin T
XRD	X-ray Diffraction

LIST OF SYMBOLS

α-helix.....Alpha helix

β-sheet.....Beta sheet

INTRODUCTION

Pancreatic cancer has one of the highest mortality rates among all cancers and has a 5-year survival rate of only 10.8% [1]. A high-throughput and non-invasive method for early detection could increases the 5-year survival rate because pancreatic cancer is often diagnosed at a late stage due to the late onset of symptoms. There is currently not a biomarker that provides adequate sensitivity and specificity for detection of early-stage pancreatic cancer. Although there have been many studies that discovered unique biomarkers to pancreatic cancer, none of these have proved to be feasible due to the high cost, time-consuming analysis, and requirement of invasive methods [2].

EVs could be an excellent candidate as a biomarker because they play critical roles within the body and carry cargo which directly reflects the state of their parent cell along with the ability to be non-invasively collected in many bodily fluids [3–11]. Recently, it had been shown that pancreatic cancer EVs were more β-sheet-rich than their healthy counterparts and an assay was developed that incorporates immunoprecipitation with β-sheet staining using Thioflavin T (ThT) fluorescent dye [12,13]. Until now, tumor-specific fluorescent staining had only been used to make accurate pancreatic cancer metastasis diagnosis and staging laparoscopy in orthotopic mouse models but not for detection purposes [14,15]. While shown as a viable detection of pancreatic cancer, immunoprecipitation and ThT staining has not been upscaled to a high throughput process in a 96-well plate.

β-sheet staining of immunocaptured exosomes has been proven successful in the detection of pancreatic cancer in a centrifuge tube but is limited by the number of samples that can be processed at a time [13]. To solve this sample processing limitation, this work aimed to create a high-throughput assay combining immunoprecipitation and ThT staining in a 96-well plate. Variations

in immunoprecipitation methodology involving antibody conjugated magnetic beads and agarose beads, or protein coated plates, were tested.

BACKGROUND

Pancreatic Cancer

Every year, pancreatic cancer takes away thousands of lives that could be saved with earlier detection. If the tumor is detected during the early stages, localized pancreatic cancer has a 5-year survival rate of 41.6%. However, the early detection of pancreatic cancer is lacking so the actual overall 5-year survival rate is only 10.8% [1]. Because of this, pancreatic cancer is considered to be one of the most malignant cancers and is the fourth leading cause of cancer deaths in the United States [16]. Moreover, the most prominent of pancreatic cancer types is Pancreatic Ductal Adenocarcinoma (PDAC), which accounts for 85% of all pancreatic cancers [17] and is resistant to chemotherapy, making it especially lethal. Thus, to increase the overall 5-year survival rate, it is important to improve the early detection of the tumor. The challenge of detecting pancreatic cancer comes from the pancreas' deep location within the abdominal cavity and late onset of symptoms. By the time symptoms begin to show it is often too late for resection of the pancreatic cancer, so alternative means for early detection are needed to increase the survival rate.

Currently, the most common clinical biomarker of pancreatic cancer is serum CA19-9, which is a carbohydrate tumor-associated antigen that is often elevated in pancreatic cancer [18]. Unfortunately, other neoplasms and diseases can cause spikes in serum CA19-9 levels, making it a less than ideal biomarker for PDAC due to a sensitivity of 70-80% and specificity below 50%. Rather than a diagnostic marker, serum CA19-9 can be employed as a treatment efficacy marker for PDAC due to its correlation to tumor size and stage [19,20]. While not perfect, CA19-9 still remains the most widely used biomarker for pancreatic cancer until a newer, more effective, biomarker is discovered [21]. Even with a more effective biomarker, it is not feasible to test the entire

population, so also knowing the risk factors are important so individuals of these groups could be screened regularly.

There are several risk factors associated with pancreatic cancer, some of which are modifiable, and some of which are non-modifiable. Of the modifiable risk factors, smoking has been shown to increase one's chance of pancreatic cancer two-fold, even after 20 years of smoking cessation [22,23]. While alcohol is not a statistically important factor in non-smokers, it was found to be a risk factor in smokers [24]. In addition to chronic alcohol use, dietary factors and obesity are also associated with an increased risk of developing pancreatic cancer, along with an increased mortality [25,26]. Awareness of these risk factors and promoting lifestyle changes can help reduce the occurrence of pancreatic cancer.

Risk factors that are beyond our control and considered to be non-modifiable are: male sex, increasing age, African-American ethnicity, and genetic mutations [27,28]. In 2012, the incident rate of pancreatic cancer was 4.9 per 100,000 in men and 3.6 per 100,000 among women [29]. Interestingly, it has been shown that there is a strong familial history linked to the rate of pancreatic cancer. The relative risk of developing pancreatic cancer is increased by a factor of 2, 6, and 30 in people with one, two, and three first-degree relatives, respectively [30]. Familial pancreatic cancer was first reported in 1967 by Lynch and his colleagues but despite numerous studies to narrow down a genetic mutation culprit, there has been little success [31,32]. One gene of interest is the germline breast cancer 2 (BRCA2) genetic abnormality which is found to be a common genetic abnormality in familial pancreatic cancer, but still only occurs in less than 20% of cases [33–35]. By identifying these risk factors of pancreatic cancer, the regular screening can be applied to improve the early detection rate.

Extracellular Vesicles

Extracellular vesicles (EVs) are an overarching term for the different populations of apoptotic bodies, microvesicles, and exosomes that are secreted by all types of cells [36]. These types of EVs differ in their contents, route of excretion, function, and size. The size ranges for apoptotic bodies, microvesicles, and exosomes are 50-5000 nm, 100-500 nm, and 50-120 nm, respectively [37,38]. It was previously shown that different diseases such as cancer, immune disorders, and infections can be associated with alterations in EV numbers and contents [39,40]. The alterations on EVs by these diseases allow them to be studied because they play important roles within the body.

Recently, it has slowly been discovered that EVs aren't a way for cells to remove unwanted contents but play many critical roles within the body [11]. It has been shown that EVs play an important role in cell to cell signaling [3–6], immune response [41], and in metastasis of cancers [42,43]. Importantly, EVs can be collected non-invasively, unlike a biopsy or surgery, from common bodily fluids like serum, saliva, semen, urine, and cerebrospinal fluid [7–10]. Along with the ability to easily collect EVs, they provide protection and stability to their contents, making them excellent candidates for new biomarker discovery.

Moreover, EVs are membrane bound by a lipid bilayer and secreted through endosomal route from their parent cell which means that their contents and surface proteins closely resemble that of their parent cells [44]. The lipid bilayer of EVs allow for stability and protection of the contents inside so that they can remain intact until they've reached the intended target. The cargo inside of EVs are proteins, DNA, RNA, and miRNA [36]. The ability to non-invasively collect EVs along with their representation of the cells state is what makes them an excellent candidate for biomarker discovery.

Protein Secondary Structure

Proteins are functional units that are made up of amino acids, which are the building blocks of proteins. The primary structure of proteins are linear chains of these amino acids. Once a primary chain is established, it folds in various patterns to form secondary structures called α-helix, β-sheet, and random coils [45]. The present methods to determine protein secondary structure are circular dichroism (CD) spectroscopy, Fourier transform infrared (FT-IR) spectroscopy, Raman spectroscopy, X-ray diffraction (XRD) spectroscopy, and nuclear magnetic resonance (NMR) spectroscopy. In each of these spectroscopies, α-helix and β-sheets show unique characteristics that allow for secondary structure determination. The table below shows the mechanism and limitation for each method [46–52].

Table 1. Comparison of methods for protein secondary structural analysis

Name	Mechanism	Limitations
XRD	Measures interference of monochromatic X-rays on a crystalline sample	High cost, exposure to X-rays, high quality samples, and time consuming
NMR	Measures absorption signals from applying electromagnetic radiation	High cost, intricate operation, and large size of equipment
FTIR/ Raman	Measures wavelength and intensity of the absorption along with characteristic bond vibrations of infrared radiation	Requires purified proteins and complex analysis needed
CD	Measures the unequal absorption of left- and right-handed circularly polarized light	High cost, purified proteins, intricate operation, and large equipment size

β-Sheet and Thioflavin T

The secondary structure of proteins is broken down into three categories, α-helix, β-sheet, and random coils. By using CD, FT-IR, and Raman spectroscopy, it has been previously shown that β-sheet levels are elevated in cancerous EVs [12,13]. Thioflavin T (ThT) is a fluorescent dye that binds strongly to β-sheets and, upon binding, has been shown to give off a strong fluorescence signal at 482 nm when it is excited at 450 nm [53–55]. In 1988, ThT was used to quantify amyloid

fibrils, β-sheet protein aggregates, and found that there was a strong linear relationship between the amyloid fibril concentration and the fluorescent intensity [56]. This ability of ThT may prove to be useful in other applications. Recently, an assay was developed utilizing ThT to simplify the measurement of β-sheet-richness and demonstrated increased fluorescence of cancer to healthy EVs [13]. This offers an alternative detection method which has the possibility of being upscaled to a high throughput assay.

METHODS

Cell Lines and Culture

Both the malignant human pancreatic cancer cell line MIA PaCa-2 and the non-malignant human pancreas cell line hTERT-HPNE were obtained from the American Type Culture Collection (Manassas, Virginia). Mia PaCa-2 cells were cultured in DMEM medium (Hyclone, GE Healthcare Life Sciences) and HPNE cells were cultured in DMEM medium (Hyclone, GE Healthcare Life Sciences) with 0.1 ng/mL epidermal growth factor (Novus Biologicals, USA). All cultures were supplemented with 10% fetal bovine serum (FBS; Life technology, Thermo Scientific Inc.), penicillin (1 U) and streptomycin (1 µg/mL). All cells were maintained in a humidified incubator with 5% CO_2 at 37 °C. All cell lines were cultured in triplicate under the same conditions and then harvested to collect independent EV samples.

Extracellular Vesicle Isolation from Culture Media

Cells were grown in culture media with serum until reached to 10^7 cells and then washed three times with phosphate-buffered saline (PBS) (pH 7.0). For collection, the cells were cultured in medium with 10% EV-depleted FBS (Thermo Scientific, US) for 48 hrs. Culture supernatants were then filtered by 0.2 µm filter and centrifuged at 10,000 g for 30 min to remove cell debris. The supernatant was then carefully centrifuged at 200,000 g for 70 min. Resulting EV precipitates were collected, dissolved in 100 µL PBS, and stored at 4 °C or -20 °C. The samples' protein contents were quantified by absorption at 280 nm in a Nanodrop ND-1000 spectrophotometer (Thermo Scientific) and diluted to desired concentration before use.

Fluorescent Spectroscopy

Thioflavin T (ThT) was obtained from Santa Cruz Biotechnology (Dallas, Texas) and diluted with PBS to a concentration of 70 µM. The concentration of ThT fluorescence was

measured at room temperature using Nanodrop. A concentration gradient (0.75 to 12 mg/mL) of Bovine Serum Albumin (BSA) was created and tested by ThT staining following the protocol: 50 µL of 70 µM ThT solution in PBS incubated with 50 µL of sample for 30 mins and then analyzed in a fluorescence plate reader (excitation 450 nm/emission 480 nm).

Immunoprecipitation and Thioflavin T Staining in a Centrifuge Tube

For the spike-in experiment, 5% of tumorous EVs were spiked into 200 µL healthy serum as case, and 200 µL healthy serum as control. 100 µL Invitrogen™ exosome human EpCAM isolation beads (Invitrogen, USA) was washed with PBS and resolved in 400 µL PBS. 200 µL serum samples and 100 µL beads were incubated for 2 hrs. at room temperature with proper shaking. After PBS wash, the beads were solved in 50 µL lysis buffer (Sigma-Aldrich, USA) for 15 min. The supernatant was collected and the protein level was then determined by evaluating absorption at 280 nm using Nanodrop. 50 µL sample and 50 µL ThT solution (70 µM) was added to 96 well plate and incubated 30 min avoiding light before reading out with the plate reader (excitation 450 nm/emission 480 nm). The final fluorescence intensity was normalized by the PBS blank with assigned ThT concentration. Comparisons between the two groups were performed using a two-tailed Student's t-test.

Immunoprecipitation and Thioflavin T Staining in a 96-Well Plate

For the spike-in experiment, 5% tumorous EVs were spiked into 200 µL healthy serum as a mimic cancer serum, and 200 µL healthy serum as control. 100 µL EpCAM conjugated biotin monoclonal antibody (Thermo Scientific, USA) was loaded onto streptavidin coated plates (Thermo Scientific, USA) (Sigma-Aldrich, USA) or Protein A/G coated plates (Thermo Scientific, USA) and incubated for 1 hr. at room temperature (RT) on an orbital mixer. After PBS wash, 200 µL serum sample was added to appropriate wells and incubated for 1 hr. at RT on orbital mixer.

Following a PBS wash, 50 µL PBS was added with 50 µL ThT solution (70 µM) into the wells and incubated for 30 min., avoiding light before reading out with the fluorescent plate reader (excitation 450 nm/emission 480 nm). The final fluorescence intensity was normalized by the PBS blank with assigned ThT concentration. Comparisons between the two groups were performed using a two-tailed Student's t-test.

RESULTS

Thioflavin T Verification

It has been previously reported that cancerous EVs are more β-sheet rich than healthy EVs and an efficient way of measuring β-sheet richness had been previously developed that incorporated immunoprecipitation and ThT staining to capture and isolate cancerous EVs [12,13]. The 5% spike of EVs from the malignant Mia cell line into the healthy human serum was performed to mimic a cancer patient's serum. There was a significant difference in fluorescent intensity between the spike and control (Fig. 1A). Thus, it was confirmed that the combination of immunoprecipitation with ThT staining worked effectively in a centrifuge tube.

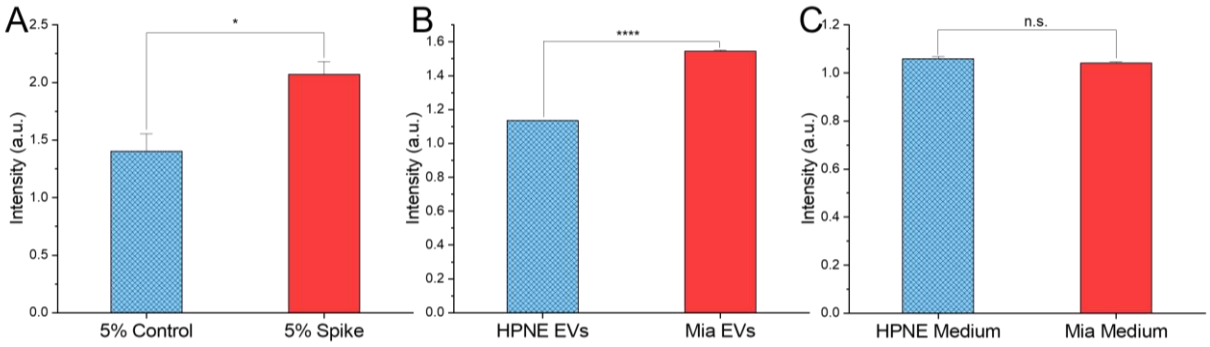

Figure 1. Thioflavin T fluorescent intensity of previously developed assay and cell culture samples.
(A) Verification of EV immunoprecipitation assay and ThT staining in a protein LoBind tube as described in previous work [13]. ThT staining of purified EVs from culture medium (B) and culture medium (C). Error bars, mean ± S.E.M.; n=3; n.s.=not significant; and $*p < 0.05$, $**p < 0.01$, $***p < 0.001$, and $****p<0.0001$.

The presence of EVs in the cell culture medium was confirmed by collecting them and putting directly into the ThT staining assay. EVs from both the malignant Mia cells and non-malignant HPNE cells were used for comparison of the β-sheet richness comparison. There was a highly significant difference between the purified HPNE and Mia EVs indicating that there is a difference in the β-sheet richness, in favor of the cancerous EVs (Fig. 1B). Since the EVs have a clear difference, it was tested whether this difference was strong enough to be present in the midst

of the background noise of other protein contaminants within the medium. Interestingly, there was not a significant difference among the two mediums tested, which indicates the need for immunoprecipitation to enrich for the cancerous EVs (Fig. 1C).

96-Well Plate Immunoprecipitation

In addition to immunoprecipitation in a centrifuge tube, it was also done in a 96-well plate. A human serum concentration gradient with ThT staining demonstrated the strong linear relationship between the number of β-sheets and the corresponding fluorescence (Fig. 2A). In order to maximize the concentration of the final sample, the minimum amount of volume needed to make a successful readout in the plate reader was used. It was determined that 100 µL of solution in the well still provided enough sensitivity for sample readings (Fig. 2B).

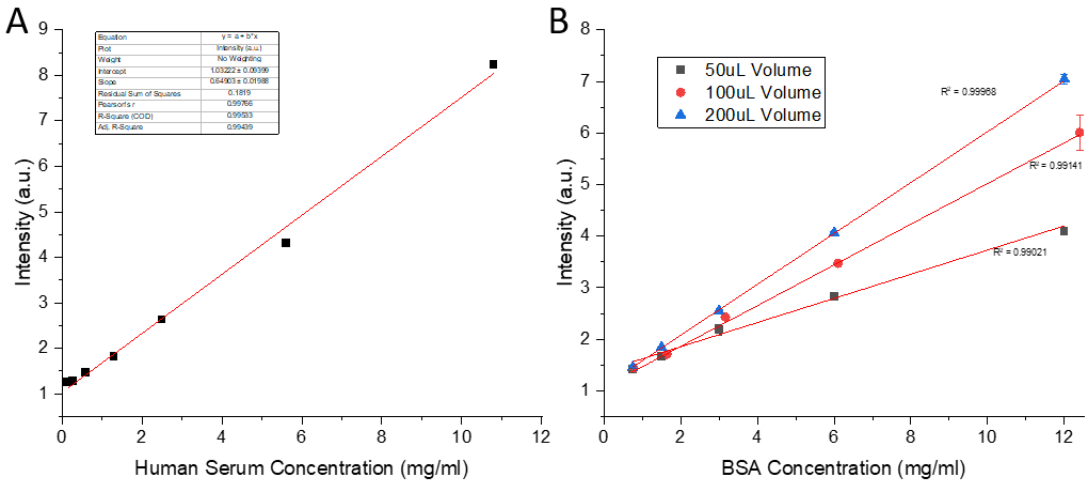

Figure 2. Scatter plot and linear regression of protein sample gradients and different well plate volumes.
(A) Scatter plot of human serum concentration gradient versus intensity after staining with Thioflavin T which shows a strong correlation (R^2=0.99533). (B) Scatter plot comparing BSA concentration gradient with different well volumes versus intensity.

With the 100 µL final well volume determined, the high throughput capabilities of immunoprecipitation and ThT staining were explored through four different methods in a 96-well plate (Fig. 3). The first method kept the same procedure as done previously in a tube, except with

performing multiple samples at once in a 96-well plate. Per the readout results, there was a 0.82% difference between the spike and control sample ($p > 0.05$) (Fig. 4A). The second method utilized a 96-well plate coated with streptavidin and EpCAM conjugated biotin monoclonal antibody was added per methods described. Streptavidin has an extremely high affinity for biotin which allows for the capture of cancerous EVs [57]. The advantage of this method is that it eliminates the need for EpCAM conjugated magnetic beads and allows for the immunoprecipitation to occur directly on the plate. However, the results of this method also showed that there was only a slight difference between the spike and control ($p > 0.5$) (Fig. 4B).

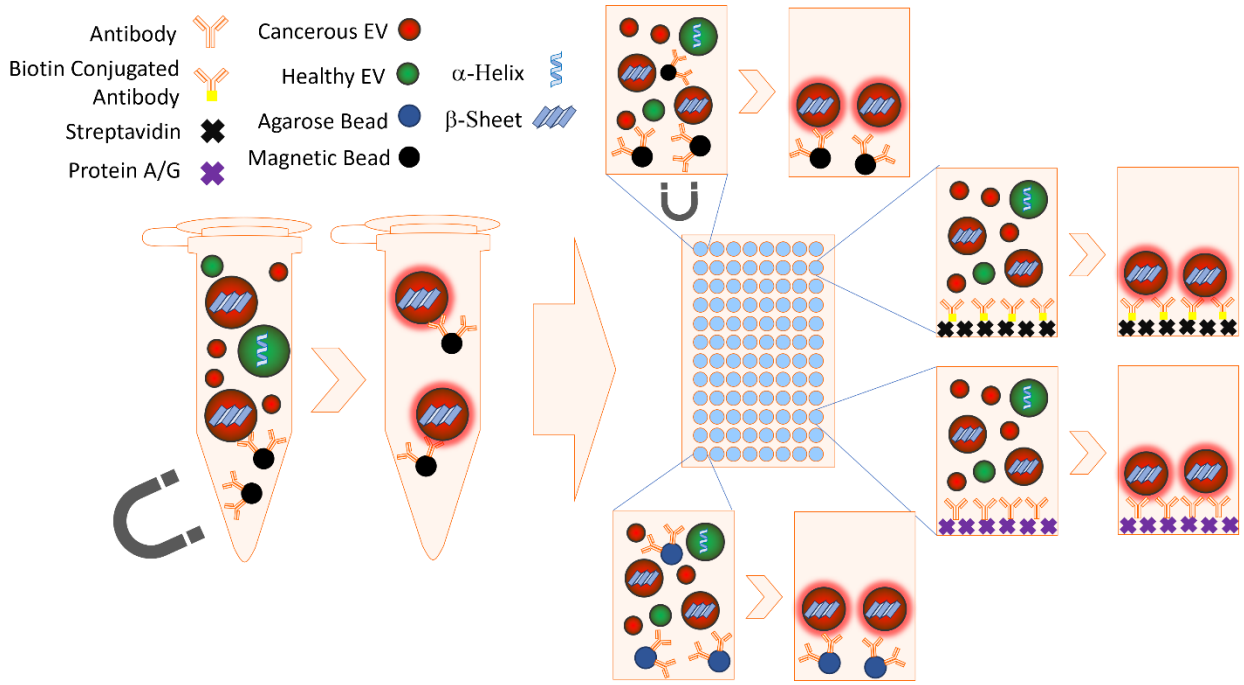

Figure 3. Schematic of immunoprecipitation with Thioflavin T fluorescent staining. Comparison of the combination of immunoprecipitation and ThT staining done in a centrifuge (top) versus in a 96-well plate (bottom).

In the third method, the setup is similar to that found in the preceding method except a combination of protein A and G was coated to the plate. Protein A and G have a strong binding affinity for monoclonal antibodies which allowed for use of unconjugated EpCAM to capture EVs [58]. The EV spike sample showed a 13.4% higher intensity, however, due to the large standard error,

the results were not significant at an alpha level of 0.05 (Fig. 4C). The last method utilized EpCAM conjugated agarose beads as an alternative to magnetic beads. The results of the experiment were unexpected with the control having a higher intensity than the spike sample (Fig. 4D).

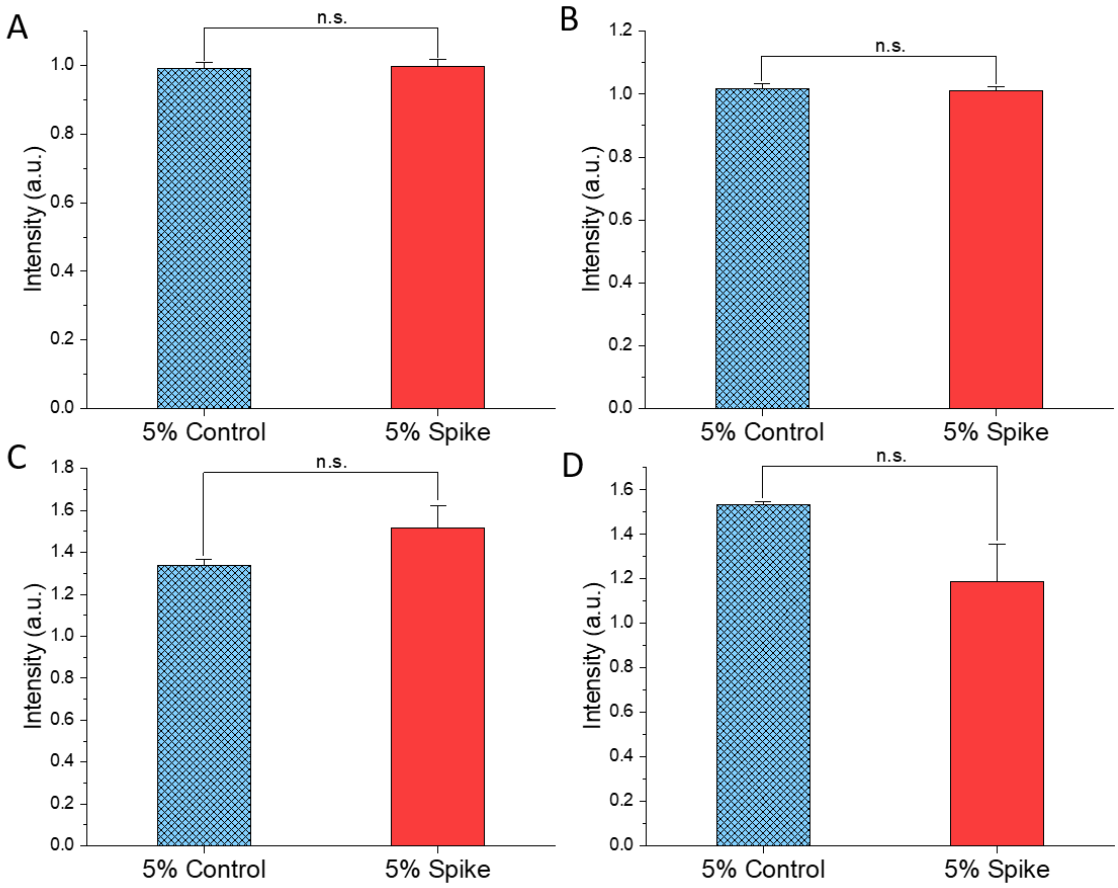

Figure 4. Thioflavin T fluorescent intensity of different 96-well immunoprecipitation methods. (A) Spike and control fluorescence using EpCAM conjugated magnetic bead immunoprecipitation in a 96-well plate. (B) Spike and control fluorescence using streptavidin coated 96-well plate with EpCAM conjugated biotin monoclonal antibody immunoprecipitation. (C) Spike and control fluorescence using Protein A/G coated 96-well plate with unconjugated EpCAM monoclonal antibody. (D) Spike and control fluorescence using EpCAM conjugated agarose beads immunoprecipitation. Error bars, mean ± S.E.M.; n=3; n.s.=not significant.

DISCUSSION

Since an immunoprecipitation reaction in a tube only allows for samples to be processed one at a time, performing immunoprecipitation and ThT staining in a 96-well plate would increase the sample processing capacity of the assay. Similar to Polymerase Chain Reaction (PCR), which allows for many samples to be processed simultaneously, upscaling from a tube to a 96-well plate allows for high throughput automation of sample processing. β-sheet staining with ThT was originally developed into a PDAC screening assay but was limited by the number of samples that could be processed at a time.

This previous assay was based on the finding that the secondary structure of proteins has a unique profile to both healthy and cancerous EVs, where EVs of malignant origin are more β-sheet rich. It was demonstrated here that there is a strong linear relationship between ThT and the amount of β-sheets present in a sample, which confirms identical findings relating to amyloid fibrils, and also shows the potential use of ThT for other applications [56]. Additionally, this research showed that the optimal volume of a sample in a 96-well plate is 100 µL, which both optimizes the plate readers ability to have a successful readout while also maximizing the EV concentration.

The combination of immunoprecipitation and ThT staining was successfully reproduced in this study which shows the ability to obtain consistent results via an ultracentrifuge tube [13]. As expected, the 5% spike sample had a higher fluorescent readout than the control sample (Fig. 1A), which is most likely due to the ability to optimize the mixing of the sample with the beads. The cell culture medium was tested to ensure that there was truly a need for the immunoprecipitation step. The immunoprecipitation step of the protocol is time consuming so the elimination of it would vastly speed up the assay. While it was confirmed that there's an increased fluorescent intensity of isolated cancerous EVs, there was no difference between the two mediums tested,

demonstrating the need for, and importance of immunoprecipitation. Knowing that a significant difference in fluorescence can be successfully obtained from a centrifuge tube, it is expected that the results could be duplicated in a 96-well plate.

Four different immunoprecipitation methods were tested in the 96-well plate setup (Fig. 3). None of the methods gave comparable results to those achieved in a centrifuge tube. Interestingly, in recent work by Mita et al., they were able to successfully perform high-throughput immunoprecipitation using agarose beads and a small target protein, in a 96-well format [59]. Contrary to their work of lysing cells and capturing a singular protein, our work aimed to trap entire exosomes during immunoprecipitation, which are a much larger size to capture.

One possible reason for the lack of intensity difference between the spike and control samples could be related to the mixing process in a 96-well plate compared to a tube. A centrifuge tube has a cap that can be securely closed, which allows for the tube to be mixed by a combination of end-over-end mixing and shaking. Unlike a tube, a 96-well plate has a cover that rests insecurely on top, preventing it from end-over-end mixing and limiting it to shaking on an orbital shaker.

Another possibility is that the fluorescent intensity of the samples was below the detection limit of the plate reader. Every piece of equipment has an upper and a lower detection limit so it is reasonable to suspect that because EVs make up such a small proportion of all the proteins in a sample, not enough EVs were captured to make an impactful reading. Regarding detection limits, it has been previously demonstrated that fluorescence microscopy has superior resolution and sensitivity over plate readers [60]. A fluorescent microscope could provide an alternative solution to measuring ThT intensity.

Although the work done here was not able to generate distinguishable results for a high-throughput pancreatic cancer screening assay that incorporates immunoprecipitation and ThT

staining in a 96-well plate, there still remains great potential for further exploration into the high throughput capabilities of this assay. An area requiring further research is creating an innovative method for providing optimal mixing within a 96-well plate. This innovative way may perhaps incorporate a snap on lid, similar to the caps seen on a centrifuge tube.

CONCLUSION

In an attempt to increase early detection of pancreatic cancer, previous research has shown that cancerous EVs are more β-sheet rich; thus, an assay measuring β-sheet richness of EVs was developed that combines immunoprecipitation and Thioflavin T staining in a centrifuge tube [12,13]. This research confirmed that an increase of ThT intensity was detected in correlation to an increase of β-sheets. This research also confirmed that the elevated β-sheet richness in cancerous EVs compared to healthy EVs can be successfully detected via this method.

This assay ideology was implemented into four different 96-well plate set-ups which used EpCAM magnetic beads, a streptavidin coated plate, a Protein A/G coated plate, and EpCAM agarose beads. Unfortunately, this work was not able to develop a method for a high-throughput assay involving immunoprecipitation and ThT staining. Possible causes for this lack of success can be related to unsatisfactory mixing, low sample concentration, and poor detection limit of the plate reader. While the experiments performed in this research yielded poor results, there remains great optimism in upscaling the capabilities of an assay involving immunoprecipitation and ThT staining. EV yields from immunoprecipitation could be increased by exploring fluorescent microscopy to provide higher sensitivity, in addition to different methods of mixing. Additionally, further experimentation regarding antibody and sample concentrations should be tested to determine the optimal concentrations needed to obtain a successful readout. All together, these improvements could lead to a high-throughput and non-invasive earlier detection of pancreatic cancer.

REFERENCES

1. NIH National Cancer Institute. Pancreatic Cancer - Cancer Stat Facts. *11/05/2019* https://seer.cancer.gov/statfacts/html/pancreas.html (2019).

2. Singhi, A. D., Koay, E. J., Chari, S. T. & Maitra, A. Early Detection of Pancreatic Cancer: Opportunities and Challenges. *Gastroenterology* **156**, 2024–2040 (2019).

3. Valadi, H. *et al.* Exosome-mediated transfer of mRNAs and microRNAs is a novel mechanism of genetic exchange between cells. *Nature Cell Biology* **9**, 654–659 (2007).

4. Hannafon, B. N. & Ding, W.-Q. Cancer stem cells and exosome signaling. *Stem Cell Investigation* **2**, 11 (2015).

5. Denzer, K., Kleijmeer, M. J., Heijnen, H. F. G., Stoorvogel, W. & Geuze, H. J. Exosome: from internal vesicle of the multivesicular body to intercellular signaling device. *Journal of Cell Science* **113**, 3365–3374 (2000).

6. Camussi, G., Deregibus, M. C., Bruno, S., Cantaluppi, V. & Biancone, L. Exosomes/microvesicles as a mechanism of cell-to-cell communication. *Kidney International* **78**, 838–848 (2010).

7. Hiemstra, T. F. *et al.* Human urinary exosomes as innate immune effectors. *Journal of the American Society of Nephrology* **25**, 2017–2027 (2014).

8. Livshts, M. A. *et al.* Isolation of exosomes by differential centrifugation: Theoretical analysis of a commonly used protocol. *Scientific Reports* **5**, (2015).

9. Muller, L., Hong, C. S., Stolz, D. B., Watkins, S. C. & Whiteside, T. L. Isolation of biologically-active exosomes from human plasma. *Journal of Immunological Methods* **411**, 55–65 (2014).

10. Yang, D. *et al.* Progress, opportunity, and perspective on exosome isolation - Efforts for efficient exosome-based theranostics. *Theranostics* **10**, 3684–3707 (2020).

11. Johnstone, R. M., Adam, M., Hammond, J. R., Orr, L. & Turbide, C. Vesicle formation during reticulocyte maturation. Association of plasma membrane activities with released vesicles (exosomes). *Journal of Biological Chemistry* **262**, 9412–9420 (1987).

12. Krafft, C. *et al.* A specific spectral signature of serum and plasma-derived extracellular vesicles for cancer screening. *Nanomedicine: Nanotechnology, Biology, and Medicine* **13**, 835–841 (2017).

13. Rasuleva, K. *et al.* β-Sheet Richness of the Circulating Tumor-Derived Extracellular Vesicles for Noninvasive Pancreatic Cancer Screening. *American Chemical Society Sensors* **6**, 4489-4498. (2021) doi:10.1021/acssensors.1C02022.

14. Tran Cao, H. S. *et al.* Tumor-specific fluorescent antibody imaging enables accurate staging laparoscopy in an orthotopic model of pancreatic cancer. *Hepato-Gastroenterology* **59**, 1994–1999 (2012).

15. Metildi, C. A. *et al.* An LED Light Source and Novel Fluorophore Combinations Improve Fluorescence Laparoscopic Detection of Metastatic Pancreatic Cancer in Orthotopic Mouse Models. *Journal of the American College of Surgeons* **214**, 997 (2012).

16. Siegel, R. L., Miller, K. D. & Jemal, A. Cancer statistics, 2019. *CA: A Cancer Journal for Clinicians* **69**, 7–34 (2019).

17. Jemal, A. *et al.* Global cancer statistics. *CA: A Cancer Journal for Clinicians* **61**, 69–90 (2011).

18. Koprowski, H., Herlyn, M., Steplewski, Z. & Sears, H. F. Specific antigen in serum of patients with colon carcinoma. *Science (1979)* **212**, 53–55 (1981).

19. Pfister, M., Gottstein, B., Kretschmer, R., Cerny, T. & Cerny, A. Elevated carbohydrate antigen 19-9 (CA 19-9) in patients with Echinococcus infection. *Clinical Chemistry and Laboratory Medicine* **39**, 527–530 (2001).

20. Liu, J. *et al.* Combination of plasma microRNAs with serum CA19-9 for early detection of pancreatic cancer. *International Journal of Cancer* **131**, 683–691 (2012).

21. Kim, H. *et al.* Biomarker panel for the diagnosis of pancreatic ductal adenocarcinoma. *Cancers (Basel)* **12**, (2020).

22. Kuzmickiene, I. *et al.* Smoking and other risk factors for pancreatic cancer: A cohort study in men in Lithuania. *Cancer Epidemiology* **37**, 133–139 (2013).

23. Pelucchi, C. *et al.* Smoking and body mass index and survival in pancreatic cancer patients. *Pancreas* **43**, 47–52 (2014).

24. Rahman, F., Cotterchio, M., Cleary, S. P. & Gallinger, S. Association between alcohol consumption and pancreatic cancer risk: A case-control study. *PLoS ONE* **10**, e0124489 (2015).

25. Berrington De Gonzalez, A., Sweetland, S. & Spencer, E. A meta-analysis of obesity and the risk of pancreatic cancer. *British Journal of Cancer 2003 89:3* **89**, 519–523 (2003).

26. Gonzalez, C. A. *et al.* Diet and cancer prevention: Contributions from the European Prospective Investigation into Cancer and Nutrition (EPIC) study. *European Journal of Cancer* **46**, 2555–2562 (2010).

27. Rawla, P., Sunkara, T. & Gaduputi, V. Epidemiology of Pancreatic Cancer: Global Trends, Etiology and Risk Factors. *World Journal of Oncology* **10**, 10–27 (2019).

28. Grover, S. & Syngal, S. Hereditary pancreatic cancer. *Gastroenterology* **139**, 1076 (2010).

29. Ilic, M. & Ilic, I. Epidemiology of pancreatic cancer. *World Journal of Gastroenterology* vol. 22 9694–9705 (2016).

30. Jacobs, E. J. *et al.* Family history of cancer and risk of pancreatic cancer: A pooled analysis from the Pancreatic Cancer Cohort Consortium (PanScan). *International Journal of Cancer* **127**, 1421–1428 (2010).

31. Lynch, H. T., Krush, A. J. & Larsen, A. L. Heredity and multiple primary malignant neoplasms: six cancer families. *The American Journal of the Medical Sciences* **254**, 322–329 (1967).

32. Shin, E. J. & Canto, M. I. Pancreatic cancer screening. *Gastroenterology* **41**, 143–157 (2012).

33. Hahn, S. A. *et al.* BRCA2 germline mutations in familial pancreatic carcinoma. *Journal of the National Cancer Institute* **95**, 214–221 (2003).

34. Couch, F. J. *et al.* The prevalence of BRCA2 mutations in familial pancreatic cancer. *Cancer Epidemiology Biomarkers and Prevention* **16**, 342–346 (2007).

35. Murphy, K. M. *et al.* Evaluation of candidate genes MAP2K4, MADH4, ACVR1B, and BRCA2 in familial pancreatic cancer: Deleterious BRCA2 mutations in 17%. *Cancer Research* **62**, 3789–3793 (2002).

36. Xu, R. *et al.* Extracellular vesicles in cancer — implications for future improvements in cancer care. *Nature Reviews Clinical Oncology* **15** 617–638 (2018).

37. Kowal, J. *et al.* Proteomic comparison defines novel markers to characterize heterogeneous populations of extracellular vesicle subtypes. *Proceedings of the National Academy of Sciences of the United States of America* **113**, E968–E977 (2016).

38. Borges, F. T., Reis, L. A. & Schor, N. Extracellular vesicles: Structure, function, and potential clinical uses in renal diseases. *Brazilian Journal of Medical and Biological Research* vol. 46 824–830 (2013).

39. Lener, T. *et al.* Applying extracellular vesicles based therapeutics in clinical trials - An ISEV position paper. *Journal of Extracellular Vesicles* **4**, 30087 (2015).

40. Nana-Sinkam, S. P., Acunzo, M., Croce, C. M. & Wang, K. Extracellular vesicle biology in the pathogenesis of lung disease. *American Journal of Respiratory and Critical Care Medicine* **196** 1510–1518 (2017).

41. Nazimek, K. *et al.* Macrophages play an essential role in antigen-specific immune suppression mediated by T CD8+ cell-derived exosomes. *Immunology* **146**, 23–32 (2015).

42. Sung, B. H., Ketova, T., Hoshino, D., Zijlstra, A. & Weaver, A. M. Directional cell movement through tissues is controlled by exosome secretion. *Nature Communications* **6**, 1–14 (2015).

43. Costa-Silva, B. *et al.* Pancreatic cancer exosomes initiate pre-metastatic niche formation in the liver. *Nature Cell Biology* **17**, 816–826 (2015).

44. Bobrie, A., Colombo, M., Raposo, G. & Théry, C. Exosome Secretion: Molecular Mechanisms and Roles in Immune Responses. *Traffic* **12** 1659–1668 (2011).

45. Petsko, G. A. & Ringe, D. *Protein structure and function*. (New Science Press, 2004).

46. Mihály, J. *et al.* Characterization of extracellular vesicles by IR spectroscopy: Fast and simple classification based on amide and C-H stretching vibrations. *Biochimica et Biophysica Acta - Biomembranes* **1859**, 459–466 (2017).

47. Yang, H., Yang, S., Kong, J., Dong, A. & Yu, S. Obtaining information about protein secondary structures in aqueous solution using Fourier transform IR spectroscopy. *Nature Protocols* **10**, 382–396 (2015).

48. Rygula, A. *et al.* Raman spectroscopy of proteins: A review. *Journal of Raman Spectroscopy* **44** 1061–1076 (2013).

49. Miles, A. J. & Wallace, B. A. Circular dichroism spectroscopy of membrane proteins. *Chemical Society Reviews* **45** 4859–4872 (2016).

50. Greenfield, N. J. Determination of the folding of proteins as a function of denaturants, osmolytes or ligands using circular dichroism. *Nature Protocols* **1**, 2733–2741 (2007).

51. Warren, B. E. *X-ray Diffraction*. (Courier Corporation, 1990).

52. Hore, P. J. *Nuclear magnetic resonance*. (Oxford University Press, 2015).

53. Xue, C., Lin, T. Y., Chang, D. & Guo, Z. Thioflavin T as an amyloid dye: fibril quantification, optimal concentration and effect on aggregation. *Royal Society Open Science* **1** (2016) doi:10.1098/rsos.160696.

54. Sulatskaya, A. I., Lavysh, A. v., Maskevich, A. A., Kuznetsova, I. M. & Turoverov, K. K. Thioflavin T fluoresces as excimer in highly concentrated aqueous solutions and as monomer being incorporated in amyloid fibrils. *Scientific Reports* **7**, 1–11 (2017).

55. Passarella, D. & Goedert, M. Beta-sheet assembly of Tau and neurodegeneration in Drosophila melanogaster. *Neurobiology of Aging* **72**, 98–105 (2018).

56. Naiki, H., Higuchi, K., Hosokawa, M. & Takeda, T. Fluorometric determination of amyloid fibrils in vitro using the fluorescent dye, Thioflavin T. *Analytical Biochemistry* **177**, 244–249 (1989).

57. Weber, P. C., Ohlendorf, D. H., Wendoloski, J. J. & Salemme, F. R. Structural origins of high-affinity biotin binding to streptavidin. *Science* **243**, 85–88 (1989).

58. Akerström, B., Brodin, T., Reis, K. & Björck, L. Protein G: a powerful tool for binding and detection of monoclonal and polyclonal antibodies. *The Journal of Immunology* **135**, 2589–2592 (1985).

59. Mita, P. *et al.* Fluorescence ImmunoPrecipitation (FLIP): A Novel Assay for High-Throughput IP. *Biological Procedures Online* **18**, (2016).

60. Meijer, M., Hendriks, H. S., Heusinkveld, H. J., Langeveld, W. T. & Westerink, R. H. S. Comparison of plate reader-based methods with fluorescence microscopy for measurements of intracellular calcium levels for the assessment of in vitro neurotoxicity. *NeuroToxicology* **45**, 31–37 (2014).